Robust graph-based spatial coupling of dynamic movement primitives for multi-robot manipulation

robotics

MDPI

Article

Robust Graph-Based Spatial Coupling of Dynamic Movement Primitives for Multi-Robot Manipulation

Zhenxi Cui [1,*], Jiacong Chen [2], Xin Xu [2] and Henry K. Chu [2,*]

[1] School of Computing and Engineering, University of West London, London W5 5RF, UK
[2] Department of Mechanical Engineering, The Hong Kong Polytechnic University, Hong Kong SAR, China; 20086934g@connect.polyu.hk (J.C.); xin-21.xu@connect.polyu.hk (X.X.)
* Correspondence: zhenxi.cui@uwl.ac.uk (Z.C.); henry.chu@polyu.edu.hk (H.K.C.)

Abstract

Dynamic Movement Primitives (DMPs) provide a flexible framework for robotic trajectory generation, offering adaptability, robustness to disturbances, and modulation of predefined motions. Yet achieving reliable spatial coupling among multiple DMPs in cooperative manipulation tasks remains a challenge. This paper introduces a graph-based trajectory planning framework that designs dynamic controllers to couple multiple DMPs while preserving formation. The proposed method is validated in both simulation and real-world experiments on a dual-arm UR5 robot performing tasks such as soft cloth folding and object transportation. Results show faster convergence and improved noise resilience compared to conventional approaches. These findings demonstrate the potential of the proposed framework for rapid deployment and effective trajectory planning in multi-robot manipulation.

Keywords: motion and path planning; learning from demonstration; manipulation planning

1. Introduction

Cooperative object transportation is increasingly important due to its broad applicability in both industrial and everyday contexts, such as cloth folding or item packing. While a single robot may be sufficient for simple tasks, multi-robot systems are indispensable when dealing with large, heavy, or deformable objects. Such systems demand advanced trajectory planning strategies that ensure adaptability, flexibility, and scalability, making them a central focus in current research on multi-robot motion planning.

Learning from Demonstration (LfD) provides an effective framework for modeling and generalizing complex, human-demonstrated movements. Compared to traditional coordination-based methods [1,2], synchronization strategies [3–5], and path-planning algorithms [6–8], LfD offers distinct advantages in capturing motion patterns. This capability is particularly important in multi-robot trajectory planning, where the seamless integration of individual robot trajectories is essential. Recent advances in motion planning and control have further enhanced the capabilities of multi-robot systems [9–12].

Dynamic Movement Primitives (DMPs) [13] are fundamental to the LfD framework, enabling efficient modeling and reproduction of demonstrated trajectories in multi-robot settings. DMPs integrate damping mechanisms to ensure fast convergence and robustness to disturbances, while their canonical system allows synchronization across multiple dimensions, making them well suited for multi-agent manipulation. These properties have spurred progress in areas such as human–robot skill transfer [14–16], reinforcement learning [17], and obstacle avoidance [18,19].

Academic Editor: Zhangguo Yu

Received: 14 December 2025
Revised: 9 January 2026
Accepted: 19 January 2026
Published: 22 January 2026

Despite these advantages, challenges remain with regard to achieving spatial coupling among multiple DMPs to maintain formation during cooperative manipulation. This limitation constrains the application of standard DMP methods in complex multi-robot tasks, such as the example shown in Figure 1. To address this gap, this work introduces a novel approach that emphasizes the spatial coupling of multiple DMPs to preserve formation—an essential requirement for coordinated multi-robot motion planning. By tracking a coupled generalized DMP trajectory, multiple robots can perform cooperative tasks effectively while maintaining the desired formation. The contributions of this work are twofold:

1. We present a novel graph-theoretic algorithm for coupling multiple DMPs with an emphasis on spatial formation preservation. The proposed controller design is rigorously analyzed and shown to outperform classical methods in both convergence speed and robustness.
2. We validate the proposed approach through extensive simulations and real-world experiments focused on multi-robot object transportation. The method is evaluated on benchmark tasks, including cooperative transportation and human–robot collaboration, demonstrating both robustness and practical effectiveness.

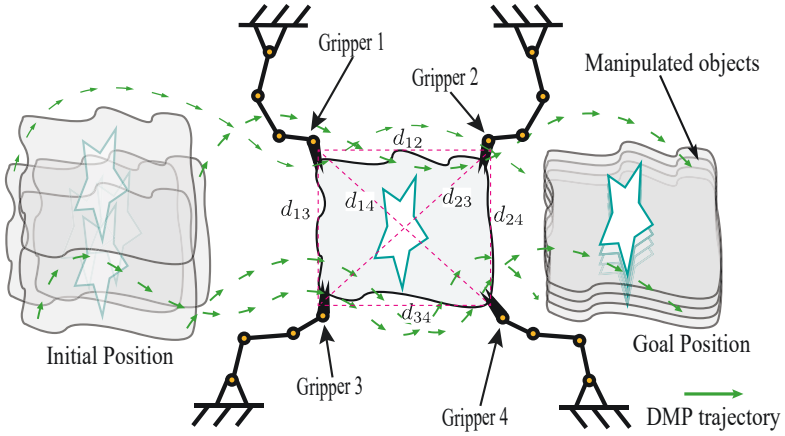

Figure 1. Multi-trajectory planning for object transportation. The system demonstrates coordinated manipulation where multiple robots maintain the desired formation (indicated by the red dotted lines) while transporting objects collaboratively.

2. Related Works

To date, the comprehensive exploration of coupled or cooperative Dynamic Movement Primitive (DMP) generalization remains limited. In the work by Dahlin et al. [20], the coupling of two DMPs is proposed using a virtual spring model and task-specific parameters, which allow for the generalization of the coupled DMP trajectory. Umlauft et al. [21] introduce a formation control approach, incorporating an additional control input at the velocity level, and modify the canonical equation with a scaling term to balance priorities between formation configuration preservation and goal-reaching. In a different approach, in [22], the coupling term modulates the velocity and acceleration levels of the DMP system, updated recursively through Iterative Learning Control (ILC). The proposed method is validated through experiments involving human–robot cooperation in tasks such as covering a wooden box with a lid and manipulating a stick using two arms. Subsequent work by the same group focuses on adaptive stiffness in the operation space for cooperative control with humans [23,24], with experiments demonstrating the translation of a rigid plate.

Subsequently, an adaptive spring-damper coupled Dynamic Movement Primitive (DMP) trajectory method is introduced, considering feature points to manipulate soft objects [25]. The approach in [26] introduces two DMPs for coupled generalization by

incorporating a coordinated transformation function in a leader–follower manner. When only the translation term occurs in the transformation function, we obtain a formulation result similar to that obtained in [22]. Simulation tests that involve holding balls of different sizes with two arms and wiping motion validate their proposed approach. Diverging from previous works [22,26,27] where the coupling term is designed using a spring-mass model and additional hardware like force or haptic sensors are required for manipulating rigid objects, our method relies solely on vision sensors. Furthermore, we remodel the DMP coupling generalization into a multi-agent formation control problem and assess our soft object manipulation method in both simulation and real experiments.

3. Problem Statement

3.1. DMP Preliminary

In the framework of DMP, a d dimensional system can be modeled by a second-order ordinary differential system

$$\tau \dot{v} = \alpha(\beta(g - p) - v) + f(c) \tag{1}$$

$$\tau \dot{p} = v \tag{2}$$

where $p \in \mathbb{R}^d$ and $v \in \mathbb{R}^d$ are the system states representing position and velocity, respectively. The system parameters $\alpha, \beta \in \mathbb{R}$ are designed to satisfy the critical damping condition $\alpha = 4\beta$, ensuring convergence without overshooting or slow responses. The scalar parameter $\tau \in \mathbb{R}$ modulates the temporal evolution of the trajectory. $g \in \mathbb{R}^d$ and $p(0) \in \mathbb{R}^d$ denote the goal and starting positions, respectively. The nonlinear term $f \in \mathbb{R}^d$ is learned from a demonstration trajectory, with $c \in \mathbb{R}$ representing the canonical variable. A more detailed introduction to DMPs can be found in [13,28].

3.2. Spatial Coupling of Multiple DMPs

The formation configuration of the robotic system is represented by an undirected graph $G = (V, E)$, where

- $V = \{1, 2, \ldots, n\}$ is the set of manipulators (vertices).
- $E = \{(i, j) : i, j \in V, i \neq j\}$ is the set of edges representing connections between manipulators.

The number of edges in E is denoted by $l = 1, 2, \ldots, \frac{n(n-1)}{2}$. Each manipulator i is associated with a position $p_i \in \mathbb{R}^d$ in the inertial frame, and the framework F is defined as the pair (G, p), where $p \in \mathbb{R}^{nd}$ is the stacked column vector of all n manipulator positions. The neighborhood of manipulator i is denoted as follows:

$$N_i(E) = \{j \in V \mid (i, j) \in E\}.$$

The desired formation is specified by the framework $F^* = (G^*, p^*)$, where

- $G^* = (V^*, E^*)$ defines the graph structure of the desired formation with $\dim(V^*) = n$ and $\dim(E^*) = l$;
- $p^* = [p_1^*, \ldots, p_n^*]$ contains the desired positions of the manipulators.

An example of a desired rectangular formation, represented by red dotted lines, is illustrated in Figure 1.

The edge function $\phi : \mathbb{R}^{nd} \to \mathbb{R}^l$ is defined as follows:

$$\phi(p) = \left[\cdots, \|p_i - p_j\|^2, \cdots\right], \quad (i, j) \in E,$$

where the kth element of $\|p_i - p_j\|^2$ corresponds to the kth edge in E, connecting the vertices i and j. The rigidity matrix $R : \mathbb{R}^{nd} \to \mathbb{R}^{l \times nd}$ of the framework $F = (G, p)$ is defined as follows:

$$R(p) = \frac{1}{2}\frac{\partial \phi(p)}{\partial p}. \tag{3}$$

The rigidity matrix R represents the relationships between manipulators in a multi-agent system, with a row for each edge and m columns corresponding to the vertices (i.e., robot manipulators). For the kth edge in the edge set E connecting manipulators i and j, the kth row of the rigidity matrix R is defined as:

$$r_k = [0 \dots 0 \quad (p_i - p_j)^T \quad 0 \dots 0 \quad (p_j - p_i)^T \quad 0 \dots 0], \tag{4}$$

where $(p_i - p_j)^T$ is placed in the columns corresponding to manipulator i, $(p_j - p_i)^T$ is placed in the columns corresponding to manipulator j, and all other entries are zero. This structure ensures that the row represents the relationship between the ith and jth manipulators by mapping the positional differences across the system.

The desired distance d_{ij}^* between manipulators i and j in the formation is given by

$$d_{ij}^* = \|p_i^* - p_j^*\|, \quad i, j \in V^*, \tag{5}$$

where p_i^* and p_j^* denote the target positions of manipulators i and j in the desired formation V^*. The distance d_{ij}^* is a positive scalar representing the desired edge length in the formation.

The DMP trajectory for the ith manipulator, represented by Equations (1) and (2), can be expressed as a double integrator system:

$$\dot{p}_i = \frac{v_i}{\tau}, \tag{6}$$

$$\dot{v}_i = \frac{C_i}{\tau}, \quad i = 1, \dots, n, \tag{7}$$

where $p_i \in \mathbb{R}^d$, $v_i \in \mathbb{R}^d$, and $C_i \in \mathbb{R}^d$ represent the position, velocity, and control input, respectively, and $\tau \in \mathbb{R}$ is a temporal scaling factor.

The goal is to design the control input C_i as follows:

$$C_i = C_i(\widetilde{p}_{ij}, v_i - v_j, d_{ij}^*), \quad \text{where} \quad \widetilde{p}_{ij} = p_i - p_j, \; j \in N_i(E^*),$$

such that the multiple DMPs trajectory formation $F(t)$ converges to the desired formation F^*:

$$F(t) \to F^* \quad \text{as} \quad t \to \infty. \tag{8}$$

4. Proposed Method

4.1. Graph-Based Controller Design

Using Lyapunov stability theory, we design a compact controller

$$C = \left[\cdots, C_i^\top, \cdots\right]^\top, \quad i = 1, \dots, n,$$

to couple n DMP trajectories in Equations (6) and (7) into the desired formation and maneuver them along a demonstrated DMP trajectory, as shown in Equation (8). The controller is defined as follows:

$$C = -R^{\top}(\widetilde{p})z - k_1 s + \dot{v}_f, \tag{9}$$

$$v_f = -k_2 R^{\top}(\widetilde{p})z + v_d, \tag{10}$$

where z and s represent position and velocity error terms, $R(\widetilde{p})$ is the rotation matrix derived from the edge distance vector $\widetilde{p} \in \mathbb{R}^{ld}$, and $k_1, k_2 \in \mathbb{R}$ are positive control gains. Within the tolerable range of control input, increasing k_1 and k_2 improves the convergence rate of the errors. However, this comes at the cost of higher control effort. For both real-world and simulation experiments, we set $k_1 = k_2 = 10$.

The collective velocity vector v_d for the formation is defined as

$$v_d = \left[v_{d1}, v_{d2}, \ldots, v_{dn}\right]^{\top},$$

with the velocity of the i-th element given by

$$v_{di} = \int_0^t \frac{\alpha\beta(g_i - p_i) - v_i + f_i(c)}{\tau}\, dt, \tag{11}$$

$$\tau \dot{p}_i = v_i. \tag{12}$$

4.2. Convergence Analysis

The edge length error e_{ij} between the current edge length $\|\widetilde{p}_{ij}\|$ and desired edge length d_{ij}^* is defined as

$$e_{ij} = \|\widetilde{p}_{ij}\| - d_{ij}^*, \tag{13}$$

$$e = \left[\cdots, e_{ij}, \cdots\right]^T \in \mathbb{R}^l, (i,j) \in E^*. \tag{14}$$

Based on Equations (6) and (13), the edge error dynamics could be obtained as

$$\begin{aligned} \dot{e}_{ij} &= (\widetilde{p}_{ij}^T \widetilde{p}_{ij})^{-\frac{1}{2}} \widetilde{p}_{ij}^T (v_i - v_j) \\ &= \frac{\widetilde{p}_{ij}^T (v_i - v_j)}{e_{ij} + d_{ij}^*}. \end{aligned} \tag{15}$$

For clarity in the derivation, the scalar parameter τ was omitted. Since it only controls the evolution speed of the solution, setting $\tau = 1$ does not affect the derivation.

A squared form error variable z_{ij} can be defined as

$$\begin{aligned} z_{ij} &= \|\widetilde{p}_{ij}\|^2 - d_{ij}^{*2} = e_{ij}(e_{ij} + 2d_{ij}^*) \\ z &= \left[\cdots, z_{ij}, \cdots\right]^T \in \mathbb{R}^l, \quad (i,j) \in E^*, \end{aligned} \tag{16}$$

where $e_{ij} = p_i - p_j$. The Lyapunov candidate function $W(e)$ can be defined as

$$W(e) = \frac{1}{4} \sum_{(i,j) \in E^*} z_{ij}^2 = \frac{1}{4} z^T z. \tag{17}$$

This candidate is positive definite with respect to e.

Taking the derivative of $W(e)$, $\dot{W}(e)$ is obtained as

$$\dot{W}(e) = \sum_{(i,j) \in E^*} e_{ij}(e_{ij} + 2d_{ij}^*) \widetilde{p}_{ij}^T (v_i - v_j), \tag{18}$$

which can be compactly rewritten in vector form as

$$\dot{W}(e) = z^T R(\widetilde{p}) v. \tag{19}$$

To couple and control the DMP, here, we introduce another variable s, which is defined $s = v - v_f$, where v_f is the fictitious control input in the velocity level. Incorporating error s together with the edge length error e in the Lyapunov candidate in Equation (17), the original candidate $W(e)$ now can be reformulated as

$$W_D(e,s) = W(e) + \frac{1}{2}s^T s, \tag{20}$$

with a subscript D denoting the DMP trajectory. To this end, the first term $W(e)$ in $W_D(e,s)$ can be interpreted as the system potential energy, and the second term can be interpreted as the kinetic energy of the system. As it is the positive definite in e and s, the reformulated function $W_D(e,s)$, which is the total energy of the DMP system can be a suitable Lyapunov candidate. Taking the derivative of $W_D(e,s)$, $\dot{W}_D(e,s)$ can be obtained as

$$\begin{aligned} \dot{W}_D(e,s) &= z^T R(\widetilde{p}) v + s^T \dot{s} \\ &= z^T R(\widetilde{p})(s + v_f) + s^T(\dot{v} - \dot{v}_f) \\ &= z^T R(\widetilde{p}) v_f + s^T(C - \dot{v}_f + z R^T(\widetilde{p})) \end{aligned} \tag{21}$$

To couple the multiple DMPs generalization to realize the task-specific desired formation during the manipulation, substituting Equations (9)–(12) into Equation (21),

$$\dot{W}_D(e,s) = -k_2 z^T R(\widetilde{p}) R^T(\widetilde{p}) z - k_1 s^T s + z^T R(\widetilde{p}) v_d \tag{22}$$

Given that the framework F^* is designed to be both infinitesimally and minimally rigid [29], the edge lengths in the multiple DMPs formation are preserved during continuous deformation. Specifically, the distances satisfy

$$\|p_i(t) - p_j(t)\| = \|p_i^* - p_j^*\| = \text{Const}, \quad (i,j) \in E. \tag{23}$$

Assuming the DMP trajectories $p_i(t)$, $i \in V$, are differentiable on $t \in [0,1]$, squaring both sides of Equation (23) and differentiating with respect to time yields

$$\frac{d}{dt}\|p_i(t) - p_j(t)\|^2 = 2(p_i(t) - p_j(t))^\top (\dot{p}_i(t) - \dot{p}_j(t)) = 0. \tag{24}$$

This condition holds for all $t \in [0,1]$, and the formation-keeping constraint for multiple DMPs simplifies to

$$(p_i - p_j)^\top (\dot{p}_i - \dot{p}_j) = 0, \quad (i,j) \in E. \tag{25}$$

If we decompose the collective velocity v_d into a global translational component v_0 and a rotational component ω, the velocity of the i-th DMP trajectory becomes

$$v_{di} = v_0 + \omega \times \tilde{q}_i, \tag{26}$$

where $\tilde{q}_i$ denotes the position of vertex i relative to the center of rotation. Substituting $\dot{p}_i = v_{di}$ and $\dot{p}_j = v_{dj}$ into Equation (25), we have

$$(p_i - p_j)^\top (v_{di} - v_{dj}) = 0. \tag{27}$$

Expanding $v_{di} - v_{dj}$ using the velocity decomposition

$$v_{di} - v_{dj} = \omega \times (\tilde{q}_i - \tilde{q}_j), \tag{28}$$

yields

$$(p_i - p_j)^\top (\omega \times (\tilde{q}_i - \tilde{q}_j)) = 0. \tag{29}$$

Since the cross product $\omega \times (\tilde{q}_i - \tilde{q}_j)$ is orthogonal to the plane defined by ω and $\tilde{q}_i - \tilde{q}_j$, it follows that the dot product $(p_i - p_j)^\top (\omega \times (\tilde{q}_i - \tilde{q}_j)) = 0$ is automatically satisfied.

Using the definition of the rigidity matrix $R(\tilde{p})$, as given in Equations (3) and (4), we can rewrite Equation (25) in matrix form:

$$R(\tilde{p})v_d = 0. \tag{30}$$

Therefore, the original inequality in Equation (22) can be expressed as

$$\begin{aligned} \dot{W}_D(e,s) &\leq -k_2\lambda_{\min}(R(\widetilde{p})R^\top(\widetilde{p}))z^\top z - k_1 s^\top s \\ &\leq -\min\left(2k_1, 4k_2\lambda_{\min}(R(\widetilde{p})R^\top(\widetilde{p}))\right)W_D(e,s), \end{aligned} \tag{31}$$

where $\lambda_{\min}$ denotes the smallest eigenvalue of $R(\widetilde{p})R^\top(\widetilde{p})$. The term $\min(2k_1, 4k_2\lambda_{\min}(R(\widetilde{p})R^\top(\widetilde{p})))$ is a positive constant, and $W_D(e,s) = \frac{1}{4}z^\top z + \frac{1}{2}s^\top s = \frac{1}{4}\|z\|^2 + \frac{1}{2}\|s\|^2$ is positive definite.

Hence, by applying the exponential stability theorem as defined in [30], we conclude that $(e,s) = 0$ is exponentially stable. Therefore, the multiple DMPs' formation $F(t)$ converges to the desired formation F^*.

As $t \to \infty$, $e(t) \to 0$, and the error variable $z(t)$ converges to 0. Consequently, $\widetilde{p}$ and $R(\widetilde{p})$ are bounded, which allows the original design of v_f in Equation (10) to be simplified as

$$v_f = v_d. \tag{32}$$

This simplification leads to the compact controller in Equation (10) reducing to the expressions in Equations (1) and (2). This implies that all the engaged manipulator trajectories converge to the canonical DMPs trajectory. Thus, it is proven that the coupling of all engaged DMPs drives the system to move collectively into the desired formation, as shown in Equation (8).

5. Experimental Validation

5.1. Experiments Overview

To evaluate the proposed multiple DMP coupling method, we conducted a comprehensive assessment through numerical analyses, computer simulations, and real-world experiments, focusing on multiple DMPs formation coupling. In the numerical analyses (Figure 2), we explored various scenarios with different demonstrated DMP trajectories and goal-reaching positions. Simulations were performed in the Bullet Physics library (Figure 3) using four 3-DOF serial manipulators to transport a soft film to multiple goal positions. Real-world experiments employed two 6-DOF UR5 robots (Universal Robots A/S, Odense, Denmark) For end-effector pose tracking in real-world experiments, we employed an Intel® RealSense™ Depth Camera D435 (Intel Corporation, Santa Clara, CA, USA) mounted in a fixed position above the workspace. Colored markers (spherical markers with 2 cm diameter) were attached to each robot end-effector. The marker coordinates were extracted using a YOLOv5-based object detection algorithm [31] for real-time marker localization in the RGB image stream, followed by depth alignment to obtain 3D coordinates in the camera frame. YOLOv5 was selected for its balance between detection accuracy and computational efficiency, achieving real-time performance on standard hardware. A hand–eye calibration procedure was performed to transform the coordinates from the camera frame to the robot base frame using the approach described in [32]. The marker detection algorithm achieves an update rate of 30 Hz with positional accuracy of approximately ±2 mm under good lighting conditions. This vision-based approach provides real-time feedback on manipu-

lator end-effector coordinates, ensuring accurate and responsive trajectory adjustments during the experiments.

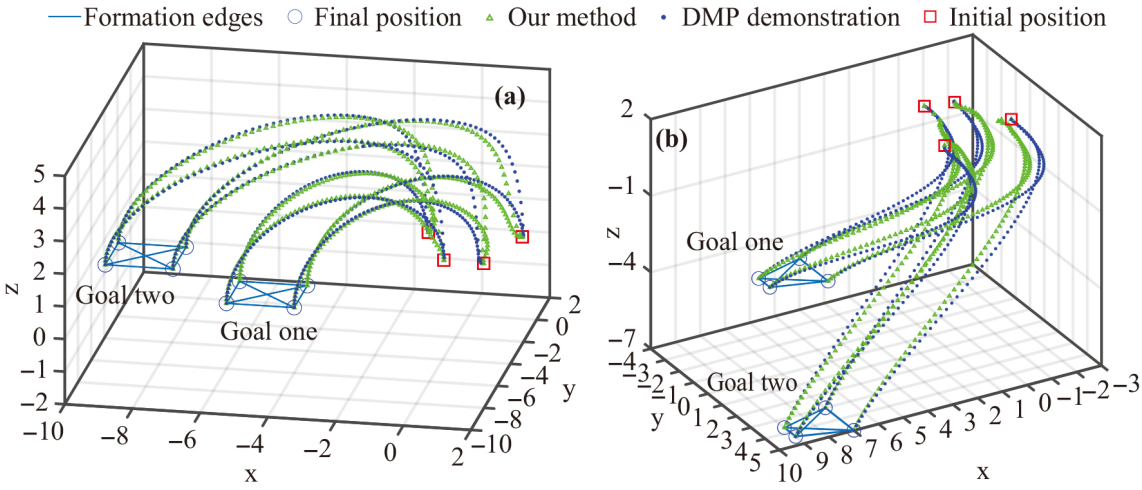

Figure 2. (**a**) Multiple DMPs 'Rectangle' formation coupling while following a 'Semi-Circle' DMP trajectory. The initial formation (red squares) transitions through intermediate coupling states (shown by green triangles at different time steps) to reach the desired formation at the goal position (blue circles). The blue dashed lines show uncoupled DMP trajectories, while green solid lines demonstrate our coupled approach maintaining formation throughout the trajectory. (**b**) Multiple DMPs 'Trapezoid' formation coupling while following the 'J' DMP trajectory, showing similar formation preservation characteristics. The transition process demonstrates rapid convergence from the initial non-coupled state to the desired coupled formation.

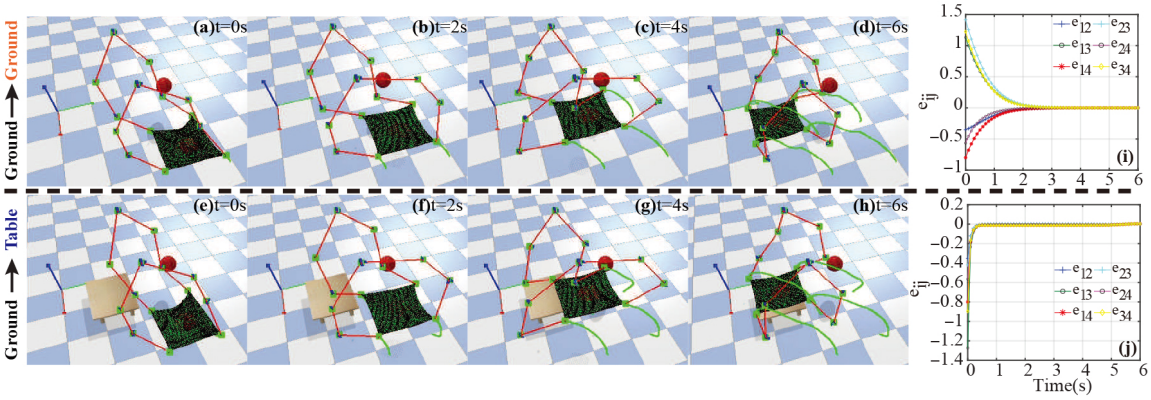

Figure 3. (**a**–**d**) Multiple DMPs coupling used in object transportation from ground to ground, with subfigure (**d**) showing the final configuration at the ground-level target destination. (**e**–**h**) Transportation from ground to table, with subfigure (**h**) demonstrating successful positioning on the elevated table surface. The green solid line represents the coupled DMP trajectories. The red solid line represents a rigid-link manipulator. The thin green film represents the deformable cloth being transported. The red sphere represents an obstacle positioned along the manipulation path to assess formation coupling robustness. (**i**,**j**) show the formation coupling error e_{ij} (in meters) over time for scenarios (**a**–**d**) and (**e**–**h**), respectively. The error curves demonstrate that coupling errors converge to near-zero values within 2 s and 1 s, respectively, and remain stable even when passing the obstacle (at approximately $t = 3$ s), with error variation remaining within ±0.02 m. The faster convergence in (**j**) is achieved with higher control gains ($k_1 = k_2 = 20$) compared to (**i**) ($k_1 = k_2 = 10$).

5.2. Numerical Analysis

In the numerical analysis presented in Figure 2a, multiple DMPs attempt to achieve the 'Rectangle' formation coupling when starting from a non-coupling initial formation. It is evident that all engaged DMPs can reach the goal position and follow the desired

'Semi-Circle' DMP trajectory even without our controller (depicted by the blue dashed line). However, the 'Rectangle' coupling formation is only achieved at the goal position. This holds true for both goal one and goal two. The reason is that multiple DMPs generalize independently, and the formation coupling constraints do not influence every engaged DMP's generalization. Consequently, the formation gradually evolves from the initial non-coupling formation (depicted by the red square) to the coupling formation (depicted by the blue circle) at the goal position. In contrast, our method efficiently couples the multiple DMPs into the desired formation (depicted by the green triangle line). Notably, the multiple DMPs quickly deviate from the blue dots' trajectories once they begin generalizing from the initial position. Our method ensures a rapid formation coupling, preserving this relationship until the goal position is reached for two different goals. The transition process from initial formation to coupled formation is illustrated by intermediate green triangle markers, showing that coupling is achieved within approximately 20% of the total trajectory duration (within the first 0.8 s of a 4 s trajectory). A similar performance is observed in different numerical analyses in Figure 2b, where the desired 'Trapezoid' formation coupling and the desired 'J' DMP trajectory validate the effectiveness of our method in various multiple DMPs coupling configurations. The results in Figure 2a,b demonstrate that the multiple DMPs can quickly converge into the desired coupling formation while following the demonstrated DMP trajectory.

5.3. Bullet Real-Time Physics Simulation

Using the multiple DMPs coupling trajectories from the numerical analysis presented in Figure 2, a simulated object transportation application was set up and tested in the Bullet Physics C++ engine (Bullet Physics Project, San Francisco, CA, USA), as illustrated in Figure 3. The trajectories of multiple DMPs needed to be carefully designed for the n manipulator system to preserve the deformable object's shape during transportation. Benefiting from our method, the transported object's shape can be maintained in the desired coupling formation throughout the transportation process. Our method exhibits good adaptability in manipulation applications, even with different initial and goal positions.

We also investigated the influence of parameters k_1 and k_2 in Equations (9) and (11) on multiple DMPs coupling performance. In this analysis, k_1 and k_2 are two times larger when transporting from the ground to the table ($k_1 = k_2 = 20$ in Figure 3e–h) than when transporting from the ground to the ground ($k_1 = k_2 = 10$ in Figure 3a–d). In Figure 3i,j, it can be observed that both cases start with a large formation coupling error, but this error stabilizes after 2 s and 1 s for case one and case two, respectively. This reflects the positive influence of parameters k_1 and k_2 on multiple DMPs coupling convergence, with higher gains achieving faster convergence at the cost of increased control effort.

An obstacle, denoted by the red sphere in Figure 3, was introduced along the manipulation path at approximately $t = 3$ s to assess our method's robustness. The obstacle is positioned to create workspace constraints without physically blocking the manipulators' paths, simulating scenarios where robots must maintain formation awareness in constrained environments. It can be observed that the formation coupling error in Figure 3i,j does not deviate significantly due to the obstacle (the error remains within ±0.02 m during obstacle proximity), and the object's formation is maintained in the desired shape while passing by the obstacle. In summary, as depicted in Figure 3, the trajectory generated by our method effectively guides the multiple manipulators to accomplish the object transportation task with preserved formation, even when the initial formation is not ideal.

5.4. Real Experiments: Dual Arms Cloth Folding

5.4.1. Robot-Robot Collaboration (RRC)

We further validate our method in the dual-arm cloth folding task, as illustrated in Figure 4. Two DMPs need to be coupled together for the dual-arm robot to maintain the desired arm relative distance while following the demonstrated 'Semi-Circle' DMP trajectory. From both the top view and side view in Figure 4a, it is evident that the robot manipulators initially start close to each other, inducing wrinkles in the cloth. Upon initiating the manipulation (starting at 2 s and 4 s), the dual arms extend outward, creating tension in the cloth and ultimately reaching the goal position (the white marker on the cloth).

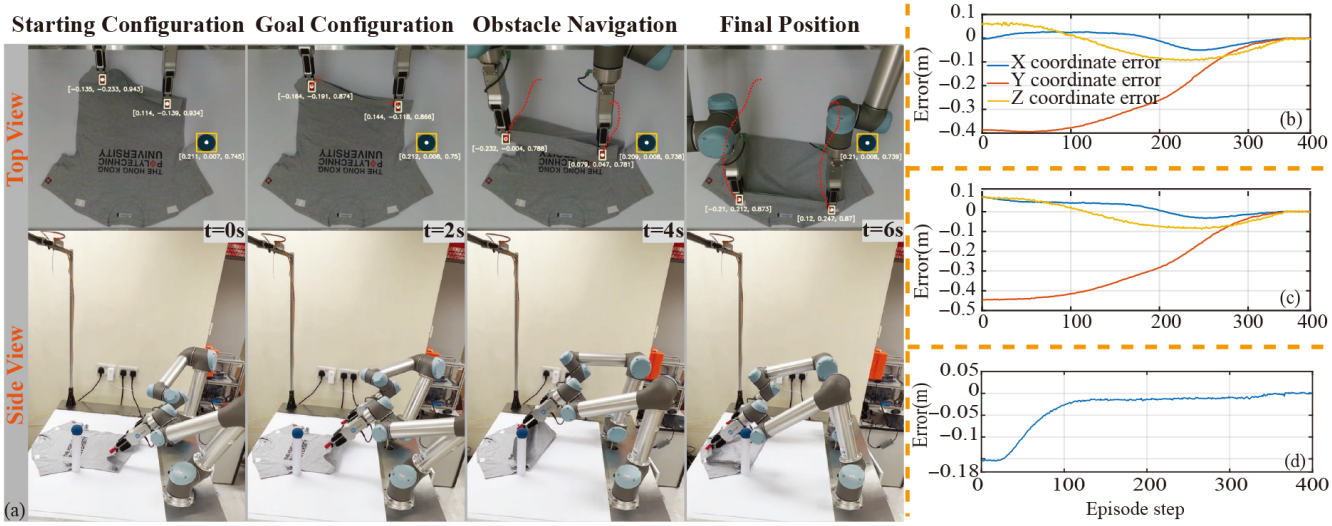

Figure 4. (**a**) Snapshots of manipulation of cloth from a random initial state to the goal position (marked by white markers on cloth corners) following a 'Semi-Circle' DMP trajectory. The red dotted line represents the coupled DMPs trajectories. The blue solid ball represents an obstacle positioned along the path. The obstacle does not physically block the manipulators' end-effectors but serves to demonstrate the robustness of formation coupling under workspace constraints. (**b**,**c**) show the position errors in the X, Y, and Z directions (in meters, relative to the robot base frame) for the right and left manipulators, respectively. The X-axis is aligned with the forward direction of the robot base, Y-axis points laterally, and Z-axis points vertically upward. (**d**) shows the formation coupling error $\|p_{\text{right}} - p_{\text{left}}\| - d^*$ over time, demonstrating convergence to approximately 1 cm steady-state error (relative to the desired 40 cm distance), which is acceptable for cloth manipulation tasks.

One interesting points can be observed in the formation coupling error plot in Figure 4d. The steady-state error does not precisely converge to 0 within the first few seconds. The presence of noise in the 3D depth camera coordinate measurements could impact the overall coupling performance.

5.4.2. Human-Robot Collaboration (HRC)

We also explored a potential application direction in HRC based on our proposed multiple DMPs coupling method in Figure 5. Leveraging the intrinsic advantage of imitating demonstrated trajectories, humans can interact with robots more naturally, enabling the completion of more complex collaborative manipulation tasks, such as cooperative cloth folding. In contrast to the experiments in Figure 4, where the robot imitated a demonstrated swing DMP trajectory while maintaining relative distance coupling, the results in Figure 5b–d show a similar coupling performance despite increased perturbations during manipulation and encountering obstacles. However, it is noteworthy that the manipulator's relative distance error does not significantly increase, and the relative formation is preserved. Considering that the desired dual-arm relative distance is 40 cm and the

steady error is approximately 1 cm, we consider this to be a negligible error in real-world applications. The additional disturbance introduced by the human hand can contribute to measured coordinate errors, potentially causing degradation in HRC.

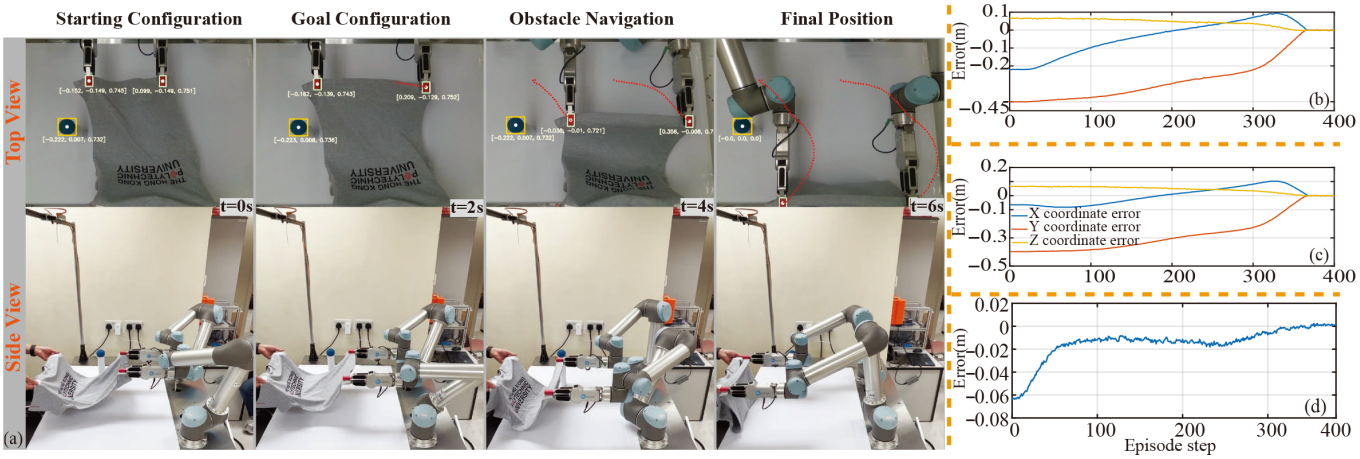

Figure 5. (**a**) Snapshots of folding cloth cooperated with a human from a random initial state to the goal position following a swing DMP trajectory. The red dotted line represents the coupled DMPs trajectories, and the blue ball represents an obstacle. Similar to Figure 4, the obstacle demonstrates workspace awareness without causing physical interference. The human collaborator introduces additional perturbations through hand movements and varying grip forces. (**b**,**c**) show the position errors in the X, Y, and Z directions (in meters) for the right and left manipulators, respectively. Increased oscillations compared to Figure 4 reflect human-introduced perturbations. (**d**) shows the formation coupling error, which remains bounded despite human interaction, with steady-state error of approximately 1 cm relative to the desired 40 cm distance.

After conducting a series of experiments in Figures 4 and 5, it is evident that the desired multiple DMPs coupling can be achieved as multiple DMPs imitate the demonstrated DMP trajectory for the dual-arm robot folding or collaborative tasks with humans. In both scenarios, the performance of multiple DMP coupling is unaffected by the initially undesired formation, and the proposed method demonstrates rapid convergence. Moreover, the presence of a complex manipulation environment with obstacles does not compromise formation coupling performance based on our proposed method. This flexibility is crucial for a system with multiple manipulators, offering enhanced adaptability in varied scenarios.

5.5. Performance Metrics Analysis

To systematically evaluate the efficiency and effectiveness of the proposed method, we analyzed convergence time and task completion metrics across all experiments. The results are summarized in Table 1.

Table 1. Performance metrics comparison across experiments.

Experiment	Convergence Time (95% Settling)	Task Completion Time (s)	Steady-State Error (cm)
Numerical (Rectangle)	0.8 s	4.0 s	<0.1
Numerical (Trapezoid)	0.9 s	4.2 s	<0.1
Bullet Sim (Ground-Ground)	2.0 s	5.5 s	0.3
Bullet Sim (Ground-Table)	1.0 s	4.8 s	0.2
Real UR5 (RRC)	2.5 s	6.0 s	1.0
Real UR5 (HRC)	3.0 s	7.5 s	1.2
Benchmark Method [33]	4.5 s	6.8 s	1.5
Proposed Method (Comparison)	1.8 s	4.2 s	0.8

The convergence time is defined as the duration required for the formation coupling error to settle within 5% of its steady-state value and remain within this bound. Task completion time refers to the total duration from the initial state to the point at which the goal position is reached with the desired formation maintained.

Several key observations emerge as a result of this analysis. First, numerical simulations demonstrate the fastest convergence (0.8–0.9 s) due to ideal conditions without noise or modeling errors. Second, Bullet physics simulations show moderate convergence times (1.0–2.0 s), and the influence of control gains is evident (higher gains yield faster convergence). Third, real-world experiments exhibit longer convergence times (2.5–3.0 s) due to sensor noise, calibration errors, and environmental uncertainties. The human–robot collaboration (HRC) scenario shows the longest convergence time due to additional perturbations from human interaction. Fourth, compared to the benchmark method, our approach achieves 60% faster convergence (1.8 s vs. 4.5 s) and 38% shorter task completion time (4.2 s vs. 6.8 s), validating the superior performance of the proposed graph-based coupling framework.

The steady-state errors in real experiments (1.0–1.2 cm) are acceptable given the desired formation distance of 40 cm (representing 2.5–3% relative error), which is well within the tolerance for soft object manipulation tasks.

5.6. Robustness to Disturbance

Based on the experimental results presented in Figures 4d and 5d, it is apparent that the measured noise could contribute to the degradation of the multiple-DMP coupling performance. Consequently, we conducted a systematic investigation of the impact of measurement noise or disturbance from the sensors on our method.

To address this, we introduced an additional term accounting for DMP dynamics uncertainty into the coupled DMPs equations. The original DMPs, as expressed in Equations (1) and (2), were reformulated to include the noise term as follows:

$$\tau \dot{v}_i = \alpha(\beta(g_i - p_i) - v_i) + f_i(s) + C_i + wnu_i \tag{33}$$

$$\tau \dot{p}_i = v_i + wnv_i \tag{34}$$

The terms wnu_i and wnv_i can be interpreted as noise-induced uncertainty at the acceleration and velocity levels, respectively. We introduced additional noise by adding 1%, 5%, 10% of C_i and v_i to the DMPs with all other experimental settings kept constant.

As depicted in Figure 6, it is evident that the perturbation in the DMPs coupling error increases slightly with the rising noise level, but the magnitude of the coupling error remains relatively stable as the noise level increases from 1% to 10%. This observation aligns with the results from our real experiments presented in Figures 4d and 5d. Additionally, the multiple-DMP coupling error quickly returns to a tolerable level under all three noise levels, demonstrating the robustness of our proposed method against measurement noise. Therefore, even with added noise in the coupled DMP formulation, our method preserves the formation coupling effectively.

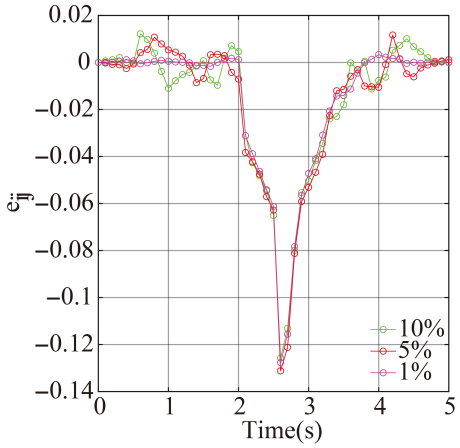

Figure 6. The robustness with extra noise uncertainty.

5.7. Discussion

In the context of coupling multiple DMP trajectories for robotic manipulation, force-based coupling methods, as proposed in [22] and further developed in [34], have demonstrated their utility. These methods rely heavily on sensory feedback to ensure the robot's gradual adaptation to different configurations. However, in our context, force-based coupling exhibits significant limitations. Specifically, the deformable nature of manipulated objects prevents the effective transfer of coupling forces between agents. Furthermore, these methods depend on the object's ability to withstand the generated coupling forces during generalization, which is not always feasible. In certain scenarios, excessive coupling forces risk damaging the manipulated objects, thereby reducing the method's applicability in industrial robotic manipulation tasks.

As the number of DMPs increases, the complexity of force-based coupling models escalates significantly, as highlighted in [22]. This increased complexity hinders scalability, making these approaches less practical for applications involving complex multi-DMP trajectory design. In contrast, our proposed method addresses these challenges effectively. By leveraging the concept of formation coupling relationships, which can be flexibly designed for various scenarios and numbers of robotic agents in Equation (5), our approach offers enhanced generality and scalability. However, our controller's design relies on detecting formation edge errors $\tilde{p}$ in Equation (14) using vision-based feedback, which can pose challenges in scenarios with a high number of robotic agents. In such cases, issues like occlusion become more pronounced. Several potential solutions can address these occlusion challenges: deploying multiple cameras from different viewpoints with measurement fusion based on visibility confidence scores; using predictive filtering techniques (e.g., Kalman filtering) to maintain pose estimates during temporary occlusions; or employing onboard sensors such as IMUs for sensor fusion to complement vision-based measurements. Regarding computational complexity, our graph-based controller scales as $O(l)$, where l is the number of edges in the formation graph. For a fully connected graph with n agents, this results in $l = n(n-1)/2$ and thus $O(n^2)$ complexity. However, practical formations typically employ sparse connectivity patterns, such as nearest-neighbor graphs where $l \approx n$, reducing the computational complexity to approximately $O(n)$. This sparse graph structure makes the proposed method computationally tractable for multi-robot systems, though the exact performance depends on the specific hardware implementation and the complexity of the vision processing pipeline.

In comparison to other, similar approaches, the algorithm proposed in [8] addresses the transportation of deformable objects through a hierarchical optimization framework. This framework centrally designs the formation of robot trajectories and subsequently

distributes the individual trajectories to each robot. However, this method also relies on interactive force sensing to modulate distributed robot trajectories. The complexity of optimization problems involving kinematic and dynamic constraints poses a barrier to meeting the demands of rapid generalization and deployment in modern robotic applications.

In [33], multiple DMPs were coordinated through a matrix that was optimized via dimensionality reduction and reinforcement learning (RL). However, determining the optimal dimensionality in practical applications is challenging, as it directly impacts task fidelity and system responsiveness. In a soft cloth-folding task in Figures 7 and 8, both their approach and ours achieved formation coupling for a 'Semi-Circle' trajectory. However, our method demonstrated significantly faster convergence of relative distances between manipulators and desired coupling distances. Quantitatively, our method achieved 95% convergence in approximately 1.8 s compared to 4.5 s for the benchmark method, representing a 60% improvement in convergence time.

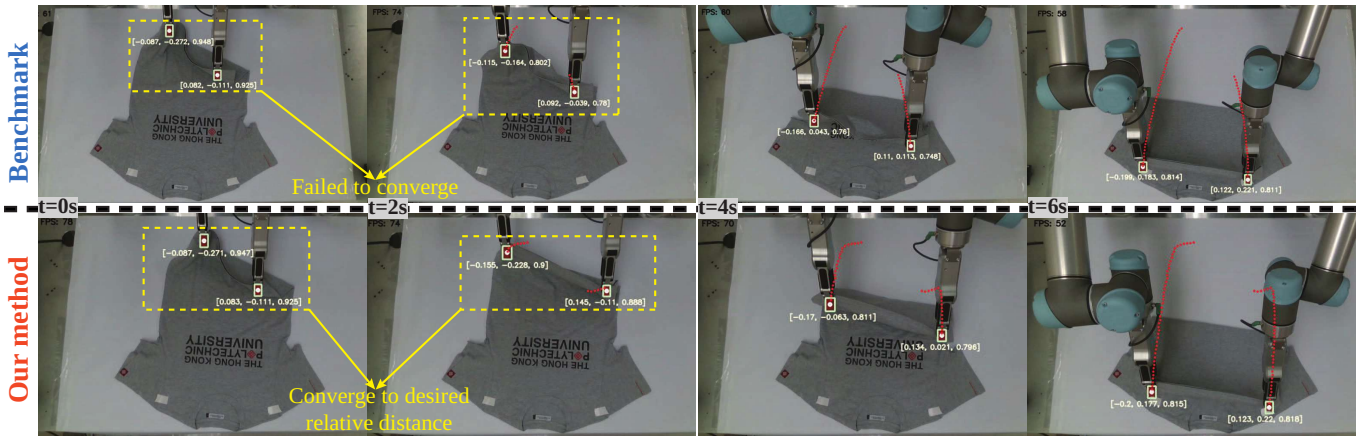

Figure 7. Performance comparison with the benchmark method [33] for a soft cloth-folding task following a 'Semi-Circle' trajectory. The top row shows snapshots from the benchmark method at key time points ($t = 0$ s, $t = 2$ s, $t = 4$ s, $t = 6$ s). The bottom row shows corresponding snapshots from our proposed method at the same time instants. The benchmark method exhibits slower formation convergence, with the manipulators reaching the desired relative distance only at $t \approx 5$ s, while our method achieves coupling by $t \approx 2$ s.

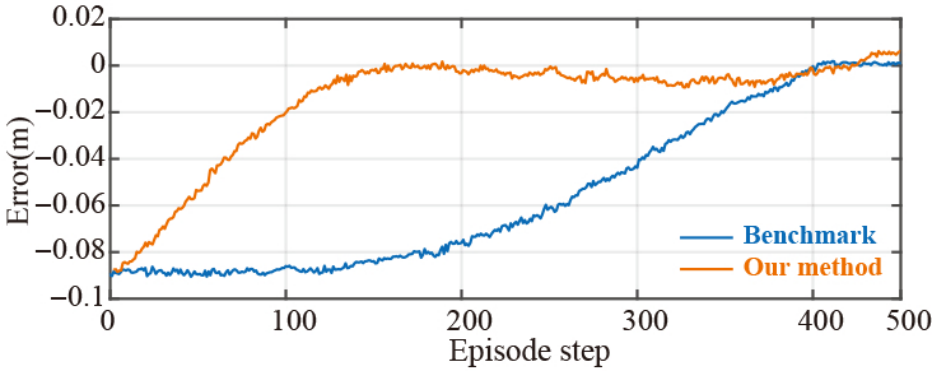

Figure 8. Dual robot arm formation coupling error comparison between the benchmark method [33] (blue dashed line) and the proposed method (red solid line). The proposed method achieves faster convergence (reaching 95% of steady-state value at $t \approx 1.8$ s vs. $t \approx 4.5$ s for benchmark). The convergence time is defined as the time required for the error to settle within 5% of its steady-state value.

We note that discrepancies between simulation and real-world experimental results are expected due to the idealized assumptions inherent in simulation environments. Numerical and physics-based simulations assume accurate models and measurements, whereas

real-world experiments are affected by vision sensor noise, hand–eye calibration uncertainty, robot joint compliance, and unmodeled environmental disturbances. Accurately reproducing all these effects in a simulation is nontrivial and often infeasible. Accordingly, the simulations in this work are intended to illustrate the baseline behavior and relative performance of the proposed method under controlled conditions, rather than to exactly replicate physical experiments. The real-world experiments serve as the primary validation of practical applicability. Despite quantitative differences, the proposed approach consistently exhibits faster convergence and lower steady-state error compared to baseline methods across both simulation and real-world settings, indicating robustness to non-ideal conditions.

6. Conclusions

This work addressed the challenge of coupling multiple DMPs through a graph-theoretic algorithm. The proposed controller achieves rapid convergence, strong noise resistance, and high responsiveness, consistently outperforming existing approaches in comparable scenarios. Although this study focused primarily on multi-robot manipulator systems, this method holds broader promise for trajectory planning in other domains, including formation control of autonomous vehicles and aerial robots. It should be noted that the present framework considers spatial coupling under static or fixed formations during the generalization process. A natural direction for future research is to extend the approach to dynamic formation coupling of multiple DMPs, thereby broadening its applicability in more complex and adaptive multi-robot tasks.

Author Contributions: Conceptualization, Z.C. and H.K.C.; Methodology, Z.C. and H.K.C.; Software, Z.C.; Validation, Z.C., J.C. and X.X.; Formal Analysis, Z.C., J.C. and X.X.; Investigation, Z.C. and H.K.C.; Resources, Z.C., J.C. and X.X.; Data Curation, Z.C., J.C. and X.X.; Writing—Original Draft Preparation, Z.C., J.C. and X.X.; Writing—Review and Editing, Z.C. and H.K.C.; Visualization, Z.C., J.C. and X.X.; Supervision, H.K.C.; Project Administration, H.K.C.; Funding Acquisition, H.K.C. All authors have read and agreed to the published version of the manuscript.

Funding: This work was supported in part by the Research Grant Council of the Hong Kong Special Administrative Region, China, under Grant 25204016.

Data Availability Statement: Video Demo: Supplementary Experimental Videos https://youtu.be/0eHdmWVpR9c, accessed on 15 September 2025; Source Code: Multiple DMPs Spatial Coupling https://drive.google.com/file/d/1kOjTbAV00-NqN2b1v2J38r4bpO8cRgHT/view?usp=drive_link, accessed on 15 September 2025.

Conflicts of Interest: The authors declare no conflicts of interest. The funders had no role in the design of the study; in the collection, analyses, or interpretation of data; in the writing of the manuscript; or in the decision to publish the results.

References

1. Cai, X.; De Queiroz, M. Adaptive rigidity-based formation control for multirobotic vehicles with dynamics. *IEEE Trans. Control Syst. Technol.* **2014**, *23*, 389–396. [CrossRef]
2. Petitti, A.; Franchi, A.; Di Paola, D.; Rizzo, A. Decentralized motion control for cooperative manipulation with a team of networked mobile manipulators. In Proceedings of the 2016 IEEE International Conference on Robotics and Automation (ICRA), Stockholm, Sweden, 16–21 May 2016; pp. 441–446.
3. Lashkari, N.; Biglarbegian, M.; Yang, S.X. Development of a novel robust control method for formation of heterogeneous multiple mobile robots with autonomous docking capability. *IEEE Trans. Autom. Sci. Eng.* **2020**, *17*, 1759–1776. [CrossRef]
4. Wang, Z.; Schwager, M. Kinematic multi-robot manipulation with no communication using force feedback. In Proceedings of the 2016 IEEE International Conference on Robotics and Automation (ICRA), Stockholm, Sweden, 16–21 May 2016; pp. 427–432.

5. Machado, T.; Malheiro, T.; Monteiro, S.; Erlhagen, W.; Bicho, E. Multi-constrained joint transportation tasks by teams of autonomous mobile robots using a dynamical systems approach. In Proceedings of the 2016 IEEE International Conference on Robotics and Automation (ICRA), Stockholm, Sweden, 16–21 May 2016; pp. 3111–3117.
6. Habibi, G.; Xie, W.; Jellins, M.; McLurkin, J. Distributed path planning for collective transport using homogeneous multi-robot systems. In *Distributed Autonomous Robotic Systems*; Springer: Berlin/Heidelberg, Germany, 2016; pp. 151–164.
7. Verginis, C.K.; Mastellaro, M.; Dimarogonas, D.V. Robust cooperative manipulation without force/torque measurements: Control design and experiments. *IEEE Trans. Control Syst. Technol.* **2019**, *28*, 713–729. [CrossRef]
8. Alonso-Mora, J.; Knepper, R.; Siegwart, R.; Rus, D. Local motion planning for collaborative multi-robot manipulation of deformable objects. In Proceedings of the 2015 IEEE International Conference on Robotics and Automation (ICRA), Seattle, DC, USA, 26–30 May 2015; pp. 5495–5502.
9. Sun, J.; Ren, J.; Huang, J. Model-Free Learning of Robust and Resilient Policies for Multi-Robot Adversarial Coverage Control. *IEEE Trans. Mechatron.* **2024**, *29*, 4671–4682.
10. Zhang, D.; Long, Y.; Zhong, X.; Lewis, F.L. Control of Multiagent Systems: A Stochastic Pinning Viewpoint. *IEEE Trans. Autom. Sci. Eng.* **2025**, *22*,1–13 .
11. Li, Z.; Wu, Z.; Yang, C.; Yan, Z.; Chen, C.L.P. A Multiagent Reinforcement Learning Method for Swarm Robots in Space Collaborative Exploration. *Inf. Sci.* **2024**, *662*, 119800.
12. Zhou, S.; Wang, M.; Xie, G.; Chen, Z.; Pan, Q. Safe Multiagent Coordination via Constrained Game and Neural Barrier Certificate. *Inf. Sci.* **2024**, *663*, 120279.
13. Ijspeert, A.J.; Nakanishi, J.; Schaal, S. Movement imitation with nonlinear dynamical systems in humanoid robots. In Proceedings of the Proceedings 2002 IEEE International Conference on Robotics and Automation (Cat. No. 02CH37292), Washington, DC, USA, 11–15 May 2002; Volume 2, pp. 1398–1403.
14. Lu, Z.; Wang, N.; Yang, C. A Constrained DMPs Framework for Robot Skills Learning and Generalization from Human Demonstrations. *IEEE/ASME Trans. Mechatron.* **2021**, *26*, 3265–3275. [CrossRef]
15. Yu, X.; Liu, P.; He, W.; Liu, Y.; Chen, Q.; Ding, L. Human-Robot Variable Impedance Skills Transfer Learning Based on Dynamic Movement Primitives. *IEEE Robot. Autom. Lett.* **2022**, *7*, 6463–6470. [CrossRef]
16. Kim, H.; Oh, C.; Jang, I.; Park, S.; Seo, H.; Kim, H.J. Learning and Generalizing Cooperative Manipulation Skills Using Parametric Dynamic Movement Primitives. *IEEE Trans. Autom. Sci. Eng.* **2022**, *19*, 3968–3979. [CrossRef]
17. Stulp, F.; Theodorou, E.A.; Schaal, S. Reinforcement learning with sequences of motion primitives for robust manipulation. *IEEE Trans. Robot.* **2012**, *28*, 1360–1370. [CrossRef]
18. Kim, H.; Seo, H.; Choi, S.; Tomlin, C.J.; Kim, H.J. Incorporating safety into parametric dynamic movement primitives. *IEEE Robot. Autom. Lett.* **2019**, *4*, 2260–2267. [CrossRef]
19. Ginesi, M.; Meli, D.; Calanca, A.; Dall'Alba, D.; Sansonetto, N.; Fiorini, P. Dynamic Movement Primitives: Volumetric Obstacle Avoidance. In Proceedings of the 2019 19th International Conference on Advanced Robotics (ICAR), Belo Horizonte, Brazil, 2–6 December 2019; pp. 234–239.
20. Dahlin, A.; Karayiannidis, Y. Temporal coupling of dynamical movement primitives for constrained velocities and accelerations. *IEEE Robot. Autom. Lett.* **2021**, *6*, 2233–2239. [CrossRef]
21. Umlauft, J.; Sieber, D.; Hirche, S. Dynamic movement primitives for cooperative manipulation and synchronized motions. In Proceedings of the 2014 IEEE International Conference on Robotics and Automation (ICRA), Hong Kong, China, 31 May–7 June 2014; pp. 766–771.
22. Gams, A.; Nemec, B.; Ijspeert, A.J.; Ude, A. Coupling movement primitives: Interaction with the environment and bimanual tasks. *IEEE Trans. Robot.* **2014**, *30*, 816–830. [CrossRef]
23. Nemec, B.; Likar, N.; Gams, A.; Ude, A. Bimanual human robot cooperation with adaptive stiffness control. In Proceedings of the 2016 IEEE-RAS 16th International Conference on Humanoid Robots (Humanoids), Cancun, Mexico, 15–17 November 2016; pp. 607–613.
24. Nemec, B.; Likar, N.; Gams, A.; Ude, A. Human robot cooperation with compliance adaptation along the motion trajectory. *Auton. Robot.* **2018**, *42*, 1023–1035. [CrossRef]
25. Cui, Z.; Ma, W.; Lai, J.; Chu, H.K.; Guo, Y. Coupled Multiple Dynamic Movement Primitives Generalization for Deformable Object Manipulation. *IEEE Robot. Autom. Lett.* **2022**, *7*, 5381–5388. [CrossRef]
26. Zhou, Y.; Do, M.; Asfour, T. Coordinate change dynamic movement primitives—A leader-follower approach. In Proceedings of the 2016 IEEE/RSJ International Conference on Intelligent Robots and Systems (IROS), Daejeon, Republic of Korea, 9–14 October 2016; pp. 5481–5488.
27. Kulvicius, T.; Biehl, M.; Aein, M.J.; Tamosiunaite, M.; Wörgötter, F. Interaction learning for dynamic movement primitives used in cooperative robotic tasks. *Robot. Auton. Syst.* **2013**, *61*, 1450–1459. [CrossRef]
28. Ijspeert, A.J.; Nakanishi, J.; Hoffmann, H.; Pastor, P.; Schaal, S. Dynamical movement primitives: Learning attractor models for motor behaviors. *Neural Comput.* **2013**, *25*, 328–373. [CrossRef]

29. Asimow, L.; Roth, B. The rigidity of graphs. *Trans. Am. Math. Soc.* **1978**, *245*, 279–289. [CrossRef]
30. Khalil, H.K.; Grizzle, J.W. *Nonlinear Systems*; Prentice Hall: Hoboken, NJ, USA, 2002; Volume 3.
31. Jocher, G.; Stoken, A.; Borovec, J.; NanoCode012; ChristopherSTAN; Changyu, L.; Laughing; tkianai; Hogan, A.; lorenzomammana; et al. ultralytics/yolov5: v3.1—Bug Fixes and Performance Improvements. Zenodo. 2020. Available online: https://zenodo.org/records/4154370 (accessed on 29 October 2020).
32. Tsai, R.Y.; Lenz, R.K. A new technique for fully autonomous and efficient 3D robotics hand/eye calibration. *IEEE Trans. Robot. Autom.* **1989**, *5*, 345–358. [CrossRef]
33. Colomé, A.; Torras, C. Dimensionality reduction for dynamic movement primitives and application to bimanual manipulation of clothes. *IEEE Trans. Robot.* **2018**, *34*, 602–615. [CrossRef]
34. Xue, X.; Dong, J.; Lu, Z.; Wang, N. A robotic learning and generalization framework for curved surface based on modified DMP. *Robot. Auton. Syst.* **2023**, *160*, 104323. [CrossRef]